COMPUTATION OF THE FLOW IN SHALLOW RIVER BENDS

J.P.Th. Kalkwijk and H.J. de Vriend

Report No 80-1

Laboratory of Fluid Mechanics
Department of Civil Engineering
Delft University of Technology

1980

Also published in the Journal of Hydraulic Research, 18 (1980), no. 4

Summary

The mathematical model presented describes the flow in rivers of which

i the depth is small compared with the width,

ii the width is small compared with the radius of curvature,

iii the horizontal length scale of the bottom variations is of the order of magnitude of the width.

Within these limits, the channel alignment can be arbitrary and it is not necessary that the width is constant. Furthermore, it is assumed that

iv the flow is mainly friction controlled,

v the longitudinal component of the velocity is predominant,

vi the Froude number is small.

The final set of differential equations accounts for the longitudinal convection (Bernoulli effect), the bottom friction, the flow curvature and the transverse convection of momentum by the secondary flow. The numerical integration procedure is straightforward and requires little computation time. Computational results are presented for a large hydraulic model which fulfils the above conditions.

CONTENTS

1. Introduction

The flow and the bed topography in curved alluvial rivers play an important part in various aspects of river engineering, such as river regulation, navigability, bank protection, dispersion of heat and polutants and the like. Hitherto, engineering problems in this field were mostly studied using hydraulic scale models. At present, however, the increased possibilities of electronic computers and the progress in numerical fluid dynamics enable the development of mathematical models of this complicated case of flow and sediment transport.
The basic idea underlying such models is that the flow can be considered quasi-stationary, i.e. the time needed for the flow to adapt to a change in the bed level is much smaller than the time needed for the bed level change itself. In that case the process of bed level development can be divided into small time intervals, during which the bed is kept fixed and the flow and the sediment transport rate are computed as if they were stationary; the corresponding rate of change of the bed level is used to predict the bed level in the next interval, etc.
Mathematical models of this kind comprise a computational procedure for steady flow in curved channels with a fixed, but arbitrary bed configuration. Two groups of such procedures have been developed, viz.

- procedures based on the integration of the depth-averaged main flow equations [1-6]; these procedures are simple and economic, but hitherto all of them disregard the convective influence of the secondary flow on the main flow; this leads to errors in the main velocity distribution, as will be shown hereafter;
- procedures based on the integration of the complete three-dimensional flow equations [7-10] ; these procedures yield good predictions of the main and secondary flow (so far only for rectangular channels, but the extension to more arbitrary geometries must be possible), but they are complicated and expensive.

The errors in the velocity predictions make procedures of the first

group unsuited for the present purpose. On the other hand, the use of a procedure of the second group, if existing at all, seems somewhat overdone for the many rivers that are shallow and have bends of moderate curvature. In that case simplifications are likely to be possible and the use of expensive fully three-dimensional flow computation methods seems to be unnecessary. A depth-averaged computation procedure including the convective influence of the secondary flow would be more appropriate then.

The present paper deals with such a depth-averaged procedure, for rivers of which:

i the depth is small compared with the width;

ii the width is small compared with the radius of curvature;

iii the horizontal length scale of the bottom variation is of the order of magnitude of the width;

iv the flow is mainly friction controlled;

v the longitudinal component of the velocity dominates the other ones;

vi the Froude number is small.

Depth-averaged balance equations for mass and momentum are derived in channel-fitted coordinates, the influence of the secondary flow on the main flow is analysed and the results of a simple, straightforward computation method are compared with experimental data.

2. Mathematical modelling

2.1. Coordinate system

Since the alignment of the river sections to be considered is curvilinear, it is rather obvious to use a curvilinear coordinate system which follows the alignment of the river. To that end the differential equations describing the conservation of mass and momentum will be formulated using a coordinate system (ψ,ϕ,z), where ψ and ϕ are orthogonal curvilinear coordinates in the horizontal plane and where the z-axis is vertical and positive in the upward direction.

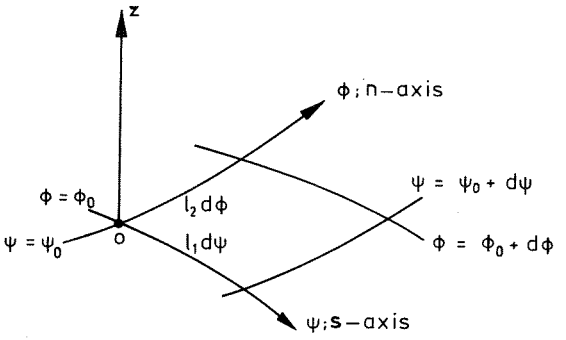

Figure 1. Coordinate system

The distance along the coordinate curves ϕ = constant and ψ = constant is indicated by s and n, respectively, and the metric functions $l_1(\psi,\phi)$ and $l_2(\psi,\phi)$ are defined such, that the length of the infinitesimal arcs ds and dn is given by

$$ds = l_1(\psi,\phi)d\psi \qquad \text{and} \qquad dn = l_2(\psi,\phi)d\phi \qquad ..(1)$$

Correspondingly, the spatial derivatives of a function $f(\psi,\phi,z)$ are

$$\frac{\partial f}{\partial s} = \frac{1}{\ell_1}\frac{\partial f}{\partial \psi};\quad \frac{\partial f}{\partial n} = \frac{1}{\ell_2}\frac{\partial f}{\partial \phi};\quad \frac{\partial f}{\partial z} = \frac{\partial f}{\partial z} \qquad ..(2)$$

If the local curvature of the s-line is taken positive when the positive n-lines diverge and inversely, these curvatures are given by (cf. [11])

$$\frac{1}{R_1} = \frac{1}{\ell_1\ell_2}\frac{\partial \ell_1}{\partial \phi} \quad \text{and} \quad \frac{1}{R_2} = \frac{1}{\ell_1\ell_2}\frac{\partial \ell_2}{\partial \psi} \qquad ..(3)$$

2.2. Governing differential equations

Without relating the horizontal coordinates to the channel geometry yet, the equation of continuity for steady incompressible flow reads (see [11] and [12]):

$$\frac{1}{\ell_1\ell_2}\frac{\partial(u_s\ell_2)}{\partial \phi} + \frac{1}{\ell_1\ell_2}\frac{\partial(u_n\ell_1)}{\partial \phi} + \frac{\partial u_z}{\partial z} = 0 \qquad ..(4)$$

, where u_s, u_n and u_z denote the velocity components in ψ- (s-), ϕ- (n-) and z-direction, respectively. Making use of (2) and (3), this equation can be rewritten as

$$\frac{\partial u_s}{\partial s} + \frac{u_s}{R_2} + \frac{\partial u_n}{\partial n} + \frac{u_n}{R_1} + \frac{\partial u_z}{\partial z} = 0 \qquad ..(5)$$

In the same way, the momentum equations can be written as

$$\frac{\partial u_s^2}{\partial s} + \frac{\partial u_n u_s}{\partial n} + \frac{\partial u_z u_s}{\partial z} + 2\frac{u_n u_s}{R_1} + \frac{u_s^2 - u_n^2}{R_2} + \frac{1}{\rho}\frac{\partial p}{\partial s} + \text{friction terms} = 0 \qquad ..(6)$$

$$\frac{\partial u_s u_n}{\partial s} + \frac{\partial u_n^2}{\partial n} + \frac{\partial u_z u_n}{\partial z} + 2\frac{u_s u_n}{R_2} + \frac{u_n^2 - u_s^2}{R_1} + \frac{1}{\rho}\frac{\partial p}{\partial n} + \text{friction terms} = 0 \qquad ..(7)$$

$$\frac{\partial u_s u_z}{\partial s} + \frac{\partial u_n u_z}{\partial n} + \frac{\partial u_z^2}{\partial z} + \frac{1}{\rho}\frac{\partial p}{\partial z} + \text{friction terms} = -g \qquad ..(8)$$

, in which p is the pressure, ρ is the mass density of the fluid and g is the acceleration due to gravity.

For small Froude numbers the water surface can be considered as if it were a rigid frictionless plate at z=0. At the fixed boundaries the usual conditions of impermeability and no-slip apply.

In shallow channels with only large-scale variations of the bed level and with gently sloping banks implying a gradual decrease of the depth to zero at the lateral bounds of the flow, the friction in vertical planes will be negligible compared with the friction in horizontal planes. Furthermore, the pressure can be assumed hydrostatic, as the convection terms and the friction terms in equation (8) will be much smaller than the pressure gradient term and the gravitation term. Taking account of these simplifications, integrating equations (5) through (7) from the bottom at z = -h(s,n) to the surface at z=0 yields (cf. [6])

$$\frac{\partial h\bar{u}_s}{\partial s} + \frac{h\bar{u}_s}{R_2} + \frac{\partial h\bar{u}_n}{\partial n} + \frac{h\bar{u}_n}{R_1} = 0 \qquad ..(9)$$

$$\frac{\partial \overline{hu_s^2}}{\partial s} + \frac{\partial \overline{hu_s u_n}}{\partial n} + 2\frac{\overline{hu_s u_n}}{R_1} + \frac{h(\overline{u_s^2}-\overline{u_n^2})}{R_2} + \frac{h}{\rho}\frac{\partial P}{\partial s} + \frac{\tau_s}{\rho} = 0 \qquad ..(10)$$

$$\frac{\partial \overline{hu_s u_n}}{\partial s} + \frac{\partial \overline{hu_n^2}}{\partial n} + 2\frac{\overline{hu_s u_n}}{R_2} + \frac{h(\overline{u_n^2}-\overline{u_s^2})}{R_1} + \frac{h}{\rho}\frac{\partial P}{\partial n} + \frac{\tau_n}{\rho} = 0 \qquad ..(11)$$

, in which the overbars denote depth-averaging; τ_s and τ_n are the s- and n-wise components of the bottom shear stress and P is the total pressure $p+\rho gz$.

2.3. Main and secondary flow

The flow pattern in river bends is known to be fairly complex: instead of moving more or less parallel to the channel axis, the fluid particles follow a helical path. This helical flow can be considered as a superposition of a more or less parallel main flow and a secondary circulation. If the orthogonal curvilinear coordinate system (s,n) is formed by the streamlines (s) and the normal lines (n) of the depth-averaged horizontal velocity field, the main flow is defined by the horizontal velocity component in the s-direction (stream-wise direction), whereas the secondary flow is defined by the horizontal component in the n-direction (normal direction).
As a first approximation. likely to hold good for the present mildly curved flows [13], the main velocity is assumed to have the logarithmic distribution along the vertical that is commonly used for uniform rectilinear shear flow:

$$u_s = \bar{u}_s \{1 + \frac{\sqrt{g}}{\kappa C} + \frac{\sqrt{g}}{\kappa C} \ln(1 + \frac{z}{h})\} = \bar{u}_s f_1(\frac{z}{h}, \frac{\sqrt{g}}{\kappa C}) \qquad ..(12)$$

A widely applied procedure to determine the horizontal component of the secondary flow, u_n, is to solve the momentum equation in the n-direction, disregarding all lateral friction terms and all inertia terms except the centrifugal one. Introducing the eddy viscosity concept for the vertical friction terms, this equation reads (see also [4] and [5])

$$-\frac{u_s^2}{R} + \frac{1}{\rho}\frac{\partial P}{\partial n} = \frac{\partial}{\partial z}(A \frac{\partial u_n}{\partial z}) \qquad ..(13)$$

, in which R_s is the local radius of curvature of the streamlines and A is the eddy viscosity.
The omission of the lateral friction terms from equation (13) corresponds with the physical idea that the depth of flow is the characteristic length scale for the turbulent processes in the

present type of flow. It implies that abrupt changes of the depth and/or the existence of vertical sidewalls cannot be accounted for. In order to make the secondary flow tend to zero at the banks, the depth should gradually approach to zero there. In addition, the streamwise inertia of the secondary flow is neglected, so that abrupt changes of the flow curvature should be avoided, as well. If all these conditions are satisfied, equation (13) holds good and the strength of the secondary flow is determined exclusively by the local properties of the main flow.
This becomes even more evident if the pressure is assumed hydrostatic and equation (13) is elaborated to

$$\frac{\partial}{\partial z}\left(A\frac{\partial u_n}{\partial z}\right) - \frac{1}{h}\left(A\frac{\partial u_n}{\partial z}\right)\Big|_{z=-h} = \frac{\overline{u_s^2} - u_s^2}{R_s} \qquad ..(14)$$

The vertical distribution of A corresponding with the logarithmic distribution of u_s in uniform rectilinear shear flow reads ([14] and [15])

$$A = -\kappa\frac{\sqrt{g}}{C} z\left(1 + \frac{z}{h}\right)\bar{u}_s \qquad ..(15)$$

As the vertical distribution of u_s in the present curved flow is taken the same as in uniform rectilinear shear flow, it is obvious to apply this parabolic distribution of A in equation (14). In that case the solution reads:

$$u_n = \frac{\bar{u}_s h}{R_s} f_2\left(\frac{z}{h}, \frac{\sqrt{g}}{\kappa C}\right) \qquad ..(16)$$

, in which f_2 is a complicated function of the vertical coordinate and the friction parameter. Figure 2 represents some of the curves according to the expression for f_2 derived by De Vriend [4, 5] as a modification of Rozovskii's theory [13].

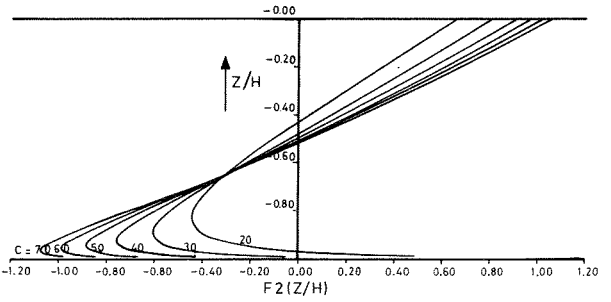

Figure 2. Secondary flow curves for various values of the friction parameter.

Experimental verification of these results is rather difficult. The few data available show that the general behaviour is predicted rather well [4, 5, 16, 17] but the magnitude seems to be somewhat underestimated [16, 17].

2.4. Analysis of the depth-averaged main flow

The (s,n) coordinate system used in par. 2.2 can be attached to the channel geometry in such a way, that the s-lines are approximately parallel to the banks and the channel axis (see also [6] and [12]). Such a choice means that the s-lines in this channel-coordinate system are rather close to the streamlines of the depth-averaged flow, so that the s-wise component of the main velocity largely dominates the n-wise one. Furthermore, if the flow is not sharply curved, the secondary flow will be small compared with the main flow, so that the following approximations will apply:

$$u_s \simeq \bar{u}_s f_1\left(\frac{z}{h}, \frac{\sqrt{g}}{\kappa C}\right) \qquad ..(17)$$

$$u_n \simeq \bar{u}_n f_1\left(\frac{z}{h}, \frac{\sqrt{g}}{\kappa C}\right) + \frac{\bar{u}_s h}{R_1} f_2\left(\frac{z}{h}, \frac{\sqrt{g}}{\kappa C}\right) \qquad ..(18)$$

, the contributions of the main and the secondary flow to u_n being of the same order of magnitude then.

Then the most important depth-averaged velocity products in equation (10) and (11) can be elaborated using (17) and (18), to

$$\overline{u_s^2} = \bar{u}_s^2 \overline{f_1^2} \simeq \bar{u}_s^2 \qquad ..(19)$$

$$\overline{u_s u_n} = \bar{u}_s \bar{u}_n \overline{f_1^2} + \frac{\bar{u}_s^2 h}{R_1} \overline{f_1 f_2} \simeq \bar{u}_s \bar{u}_n + k_{sn} \frac{\bar{u}_s^2 h}{R_1} \qquad ..(20)$$

$$\text{, where } k_{sn} = 5 \frac{\sqrt{g}}{\kappa C} - 15.6\left(\frac{\sqrt{g}}{\kappa C}\right)^2 + 37.5\left(\frac{\sqrt{g}}{\kappa C}\right)^3 \qquad ..(21)$$

A graphical representation of k_{sn} as a function of C is given in figure 3.

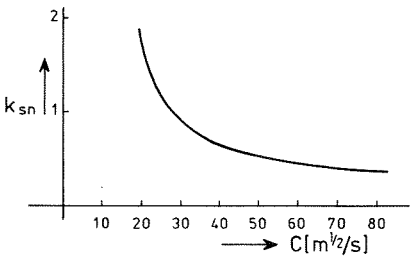

Figure 3. Factor for transverse momentum exchange by the secondary flow.

As u_n is small compared with u_s, u_n^2 will be disregarded with respect to u_s^2 in the longitudinal momentum equation (19) and all terms related to u_n, including the bed shear stress term, will be disregarded in the transverse momentum equation (11). If, in addition, the commonly used quadratic relation between the longitudinal bed shear stress and the longitudinal velocity is adopted, the depth-averaged system of equations can be written as:

$$\frac{\partial h\bar{u}_s}{\partial s} + \frac{h\bar{u}_s}{R_2} + \frac{\partial h\bar{u}_n}{\partial n} + \frac{h\bar{u}_n}{R_1} = 0 \qquad ..(9)$$

$$\bar{u}_s \frac{\partial \bar{u}_s}{\partial s} + \bar{u}_n \frac{\partial \bar{u}_s}{\partial n} + \frac{\bar{u}_n \bar{u}_s}{R_1} + \frac{k_{sn}}{h} \frac{\partial}{\partial n} \left(\frac{\bar{u}_s \bar{h}^2}{R_1}\right) + 2k_{sn} \frac{\bar{u}_s^2 h}{R_1^2} + \frac{1}{\rho} \frac{\partial P}{\partial s} + \frac{g}{C^2} \frac{\bar{u}_s^2}{h} = 0 \qquad ..(22)$$

$$- \frac{\bar{u}_s^2}{R_1} + \frac{1}{\rho} \frac{\partial P}{\partial n} = 0 \qquad ..(23)$$

So, apart from the usual terms representing the main flow inertia, the pressure gradient and the bottom shear stress, the longitudinal momentum equation contains two terms that account for the transverse exchange of main flow momentum by the secondary flow. In order to have a better insight into the role of these terms, equations (22) and (23) are combined to

$$\frac{d}{ds} \left(\frac{P}{\rho} + \frac{\bar{u}_s^2}{2}\right) = - \frac{\bar{u}_s^2}{h} \left[\frac{g}{C^2} + k_{sn} \frac{\partial}{\partial n} \left(\frac{h^2}{R_1}\right) \right] \qquad ..(24)$$

, holding along the characteristics

$$\frac{dn}{ds} = \frac{\bar{u}_n}{\bar{u}_s} + 2 k_{sn} \frac{h}{R_1} \qquad ..(25)$$

Now the effect of secondary flow convection is clearly shown. Firstly, the characteristics no longer coincide with the streamlines of the depth-averaged flow, but gradually shift towards the outer bend (if h tends to zero at the banks, they remain within the bed, the characteristics at the banks coinciding with the water line then). Secondly, the secondary flow convection causes a redistribution of the total flow energy over the cross-section, as illustrated by figure 4.

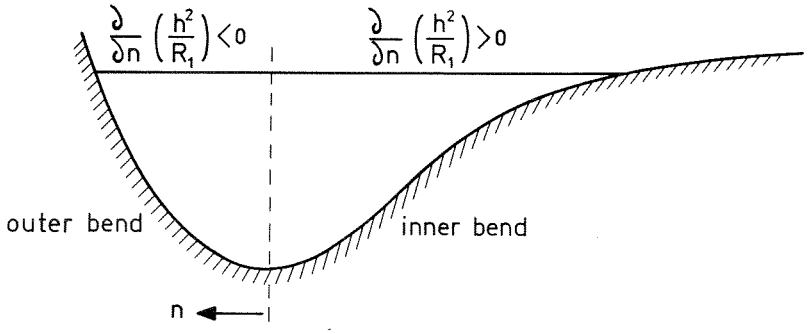

Figure 4. Influence of secondary flow convection on the total energy.

The secondary flow convection term in equation (24) is always positive in the inner part of the bend and negative in the outer part, irrespective of the sense of curvature (if the channel is curved in the opposite sense, both n and R_1 change sign in figure 4). This implies that along the characteristics (25) in the inner bend secondary flow convection tends to reduce the total energy of the flow, whereas along the ones in the outer bend the energy tends to be enhanced. Consequently the main velocity distribution tends to be skewed outwards.
Even though the secondary flow convection terms in (24) and (25) will be rather small for the bends considered here, they steadily act in the same sense and their effects accumulate. Hence the deformation of the main velocity distribution due to secondary flow convection can become considerable.
Essentially the same phenomenon, though somewhat more complicated, occurs in rectangular channel bends. Without secondary flow convection the main velocity maximum lies near the inner wall throughout the bend and in a straight reach downstream of its exit the velocity distribution soon becomes almost uniform [4, 5, 16]. If the effect of secondary flow convection is taken into account, however, an explanation can be given for the outward shift of the velocity maximum in a bend and the strongly skewed velocity distribution in a straight reach beyond it, as observed in many experiments [4, 5, 13,

16 and many others].

Equation (24) shows again that the application of the theory is limited to cases where the secondary flow convection term $k_{sn} \frac{\partial}{\partial n} (h^2/R_l)$ is not systematically (much) larger than the friction parameter g/C^2. In sharp bends, for instance, the convection term can become so large, that the term in brackets in (24) becomes strongly negative along the outer bank, which in turn can give rise to an unlimited growth of the velocity there. It is clear that in practice this will not occur because of lateral friction effects, which have been disregarded in the present analysis.

2.5. Method of integration

It seems attractive to integrate equations (9), (22) and (23) using the characteristic relations as given by expressions (24) and (25). The characteristics, however, still contain the transverse component of the main velocity $\bar{u}_n$, so that their position is not known in advance. Therefore, in order to simplify the integration procedure, a modified form of expressions (24) and (25) is used, considering the terms with $\bar{u}_n$ in equation (22) to be known. Then expression (24) changes into:

$$\frac{d}{ds} \left(\frac{P}{\rho} + \frac{\bar{u}_s^2}{2}\right) = - \frac{\bar{u}_s^2}{h} \left[\frac{g}{C^2} + k_{sn} \frac{\partial}{\partial n} \left(\frac{h^2}{R_l}\right)\right] - \left[\bar{u}_n \frac{\partial \bar{u}_s}{\partial n} + \frac{\bar{u}_n \bar{u}_s}{R_l}\right] \qquad ..(26)$$

, which is integrated along the characteristics:

$$\frac{dn}{ds} = 2\, k_{sn} \frac{h}{R_l} \qquad ..(27)$$

, meanwhile satisfying the integral condition of continuity

$$\int_{\text{width}} h\bar{u}_s \, dn = Q \qquad ..(28)$$

in each normal section of the river. Subsequently, $\bar{u}_n$ is determined from equation of continuity (9) and the computation of $\bar{u}_s$ from equations (26) through (28) is repeated, etc.
The advantage of this (iterative) procedure is, that the characteristics are no longer determined by the flow, but only by the geometry of the river as given by its depth and curvature. Moreover, in many practical cases the characteristics remain very close to the s-lines of the coordinate system because of the small values of h/R_1. In such cases the computations can be simplified even further by considering the s-lines as approximations of the characteristics (27).
In channels of constant width the s-lines can be chosen parallel to the axis, so that the n-lines will be straight and perpendicular to the axis. In that case the channel is actually discretized to a series of infinitesimal parts of circle sectors, each having its own radius of curvature and its own cross-sectional geometry.

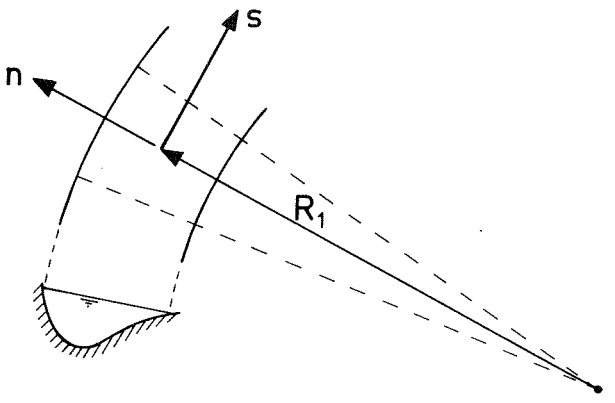

Figure 5. River-oriented coordinate system.

Equation (26) can be written as:

$$\frac{d}{ds}\,(P/\rho + U/2) = -Ua - b \qquad ..(29)$$

in which $U = \bar{u}_s^2$

$$a = \frac{g}{C^2 h} + \frac{k_{sn}}{h} \frac{\partial}{\partial n} \left(\frac{h^2}{R_1}\right)$$

$$b = \bar{u}_n \frac{\partial \bar{u}_s}{\partial n} + \frac{\bar{u}_n \bar{u}_s}{R_1}$$

Adopting a computational grid ($i\Delta s$, $j\Delta n$), this equation can be discretized to

$$\frac{1}{\rho} P[i,j+1] - \frac{1}{\rho} P[i,j] + \frac{1}{2} U[i,j+1] - \frac{1}{2} U[i,j] =$$

$$- \left[U[i,j]\ a[i,j] + U[i,j+1]\ a[i,j+1] + b[i,j] + b[i,j+1]\right]\frac{\Delta s}{2}$$

..(30)

Substracting this result from the similar result for n = (i+1) Δn yields an expression from which the quantity $\frac{1}{\rho} P|i+1,j+1| - \frac{1}{\rho} P|i,j+1|$ can be eliminated using equation (23). This leads to

$$U[i+1,j+1]\left[\frac{1}{2} + \frac{\Delta s}{2}\ a[i+1,j+1] + \frac{\Delta n}{R|i+1,j+1|}\right] =$$

$$U[i,j+1]\left[\frac{1}{2} + \frac{\Delta s}{2}\ a[i,j+1] - \frac{\Delta n}{R|i,j+1|}\right] +$$

$$U[i+1,j]\left[\frac{1}{2} - \frac{\Delta s}{2}\ a[i+1,j]\right] + U[i,j]\left[-\frac{1}{2} + \frac{\Delta s}{2}\ a[i,j]\right] +$$

$$\frac{1}{\rho} P[i+1,j] - \frac{1}{\rho} P[i,j] +$$

$$\frac{\Delta s}{2}\left[b[i,j] + b[i,j+1] - b[i+1,j] - b[i+1,j+1]\right] \qquad ..(31)$$

Starting from a given boundary value for U and assuming all quantities in the RHS to be known, $U[i,j+1]$ can be determined from this equation. Thereby the boundary value of U is chosen such that the integral continuity condition (28) is fulfilled. After the determination of the longitudinal velocity $\bar{u}_s$ in a ray, the total pressure in that ray is solved from equation (29), for instance. After sweeping through the whole flow region, all velocities $\bar{u}_s$ are known and the transverse velocities $\bar{u}_n$ can be evaluated using the equation of continuity (9). Next the coefficients b and the flow field can be computed again and as many iterations can be made as accuracy requires.
This method of integration proves to be very efficient; it does not show any instability and computer costs were low.

3. Results and discussion

The Delft University of Technology and the Delft Hydraulics Laboratory have commonly carried out experiments in a hydraulic model which fulfilled the conditions mentioned before [17]. It consisted of a straight symmetric parabolic cross-section followed by a curved part (radius 50 m), in which the deepest point of the bottom gradually shifted from the middle of the channel to the outer bend. The length of the curved part was about 80 m (fig. 6a). The areas of the wet cross-section in the straight and curved parts of the channel were about the same. Figure 6b shows the bottom configuration in detail. In the same figure the characteristics according to equation (27) are shown and they illustrate that the deviations from the s-lines will not give rise to large errors in the flow computation.
The friction coefficient of Chezy was about 60 $m^{\frac{1}{2}}/s$. Experiments were done with discharges of 0.463 m^3/s and of 0.212 m^3/s , using the same water depth. The bed of the channel had a small inclination in order to compensate for friction losses.

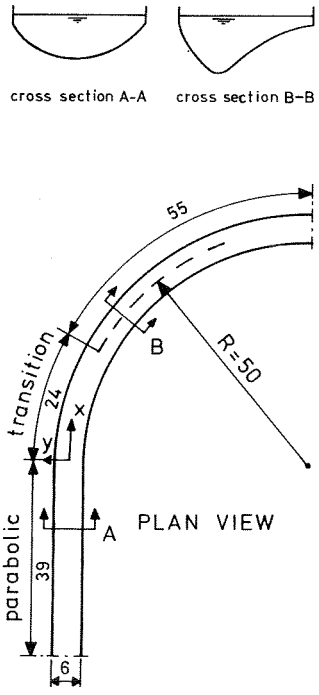

Figure 6a. Plan view of hydraulic model

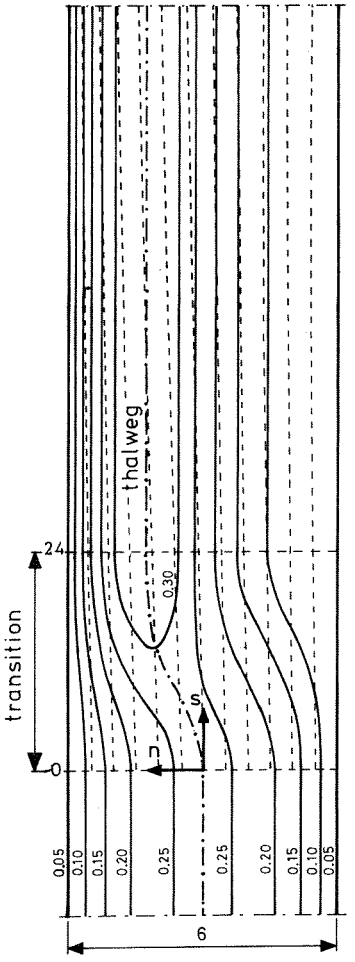

Figure 6b. Plan view of hydraulic model showing coordinate system, depth contours and characteristics

The experimental results for the velocity $\bar{u}_s$ and the total pressure (transposed to the water level) are plotted in figure 7. The velocities for the small discharge have been scaled up to those for the high discharge. This is possible because of the theoretical similarity of the velocity profiles. The pressure results are proportional to Q^2, but those of the small discharge are not represented as it appeared to be impossible to measure them accurately enough.

Figure 7 also gives the results of the mathematical model if the influence of the secondary flow on the main flow is disregarded ($k_{sn} = 0$, dashed curves). The various results give rise to the following observations.

i The similarity between the measured velocity profiles for low and high discharge is almost perfect. As a consequence, the discrepancies which can be observed between experimental and mathematical results can hardly be attributed to errors in the flow measurements (see also [18]).

ii In general the experiments and computational results for the velocity compare well. The influence of the secondary flow on the main flow is significant. As predicted by equation (24), disregarding the influence of the secondary flow leads to higher velocities in the inner bend and to lower velocities in the outer bend. As was shown by Rozovskii [13], this effect is even more pronounced if the channel cross-section has the same symmetric (i.c. parabolic) shape throughout the flume.

iii In the outer bend a systematic discrepancy between the experimental and the theoretical velocity profiles can be observed: the measured velocities close to the outer bank are higher than predicted. Three reasons for this deviation can be mentioned. Firstly, the theory tends to underestimate the secondary flow. The differences amount a factor 1.5 [17]. Therefore the computation is repeated with the coefficient k_{sn} multiplied by 1.5. In figure 8a the results of this computation are compared

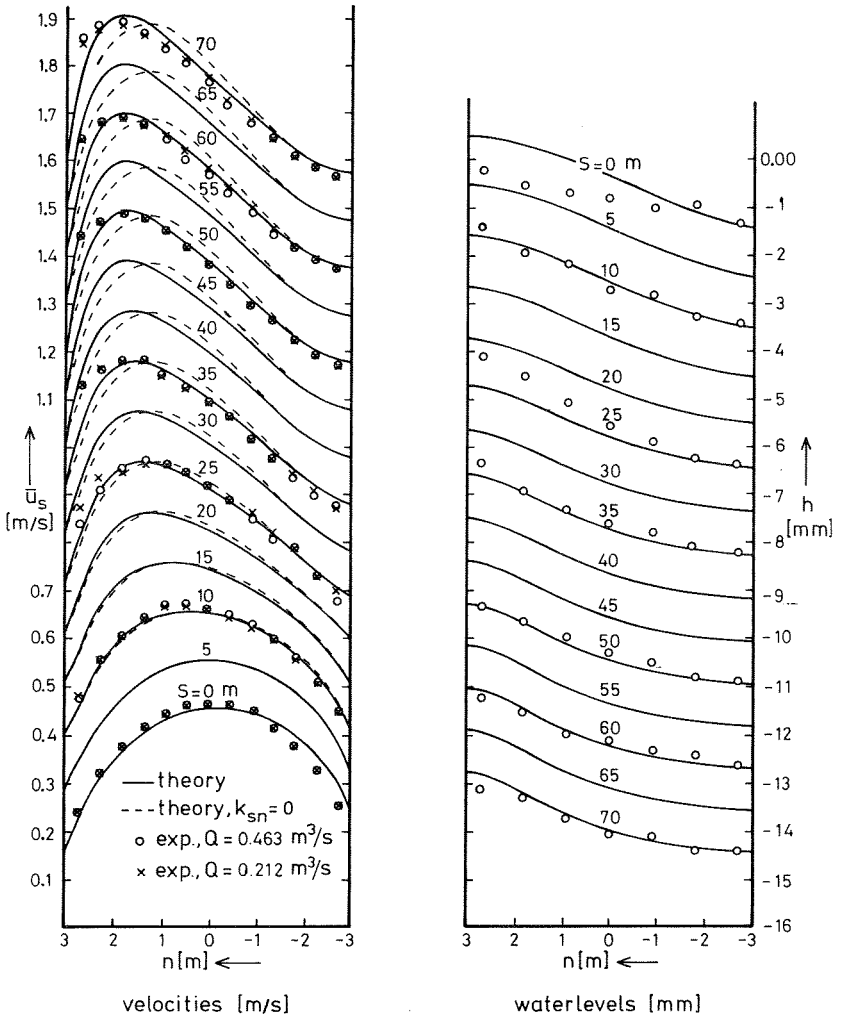

Figure 7. Theoretical and experimental results for velocities and water levels

with the original ones. The picture shows a further increase of the velocities in the outer bend and a further decrease in the inner bend, indeed. Secondly, the computation is based upon the approximation of the characteristics by the s-lines. The consequence is, that the shift of the characteristics to the outer bend is not reproduced. According to fig. 6 this shift is not very large, but nonetheless it is a systematic effect. Thirdly, the underwater bank in the outer bend has a slope of 1:3, which is rather steep. The derivations are based on a gradual change of the depth without stating explicitly what rate of change of the depth is permissible. Possibly, the slope is already too steep, which would imply that the secondary flow is no longer determined by the local flow properties alone.

iv Another discrepancy between the measured and theoretical velocity profiles occurs at the beginning of the transition (s=0). The measured velocity is somewhat overestimated there. This caused by the sudden change of curvature as used in the computation, whence s=0 m the horizontal water level suddenly gets a transverse slope. Because of the Bernoulli effect the theoretical velocity becomes somewhat higher in the inner bend and somewhat lower in the outer bend. In the next steps this effect disappears.

v Similar effects can be observed in the results for the pressure. At s=0 m the measured fall between outer and inner bend is lower than predicted. Obviously the curvature of $1/50\ m^{-1}$ is not yet reached there. Furthermore, the theoretical pressure result at s=25 m is also less satisfactory. This must be attributed to the effect of the transition in the bottom configuration between s=0 m and s=25 m. Near the end of this transition, the curvature of the thalweg, and hence of the streamlines is higher than the curvature of the s-lines, so that the transverse pressure gradients will be higher than predicted. In fact it is not very difficult to include the local flow curvature (to be derived from the flow field in the subsequent iteration steps [4] in the numerical

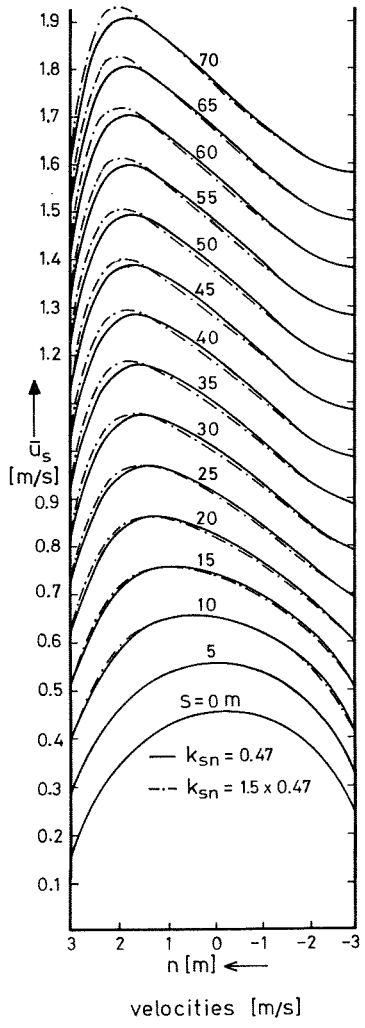

Figure 8a. Influence of the strength of the secondary flow on the main flow

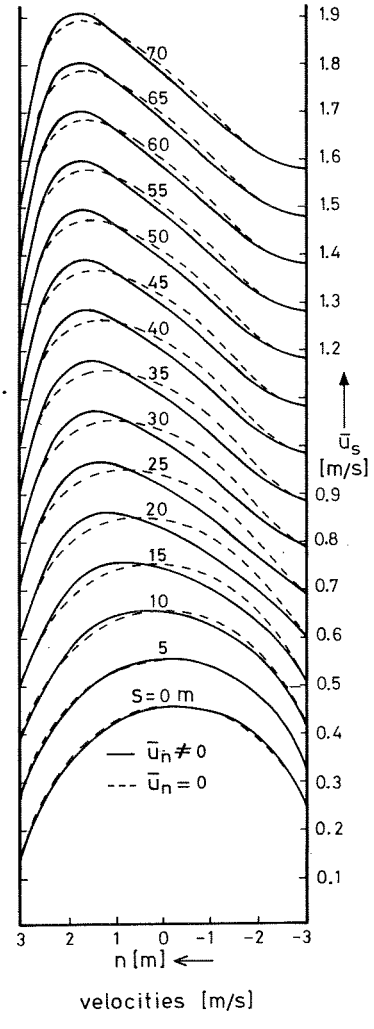

Figure 8b. Influence of the transverse main velocity

programme. As yet this has not been attempted since the velocity profiles are considered satisfactory.

vi In the derivation of the final equations (24) and (25) the influence of the resulting cross-flow was explicitly taken into account. That this is important is illustrated by fig. 8b, showing what happens to the velocities if in equation 29 the quantity b is set equal to zero. In particular in the transition the differences are relatively large. Hence it must be concluded that this effect cannot be disregarded.

4. Conclusion

Steady flow in shallow rivers of moderate curvature and with gradual depth changes can be adequately described by shallow water equations, provided that the extra terms accounting for transverse momentum exchange due to the secondary flow are introduced in the equation(s) of motion. These additional terms are related to the square of the main velocity, the flow curvature and the transverse change of the bottom level. In the characteristic relation (24) their influence can be compared directly with the influence of friction. Accounting for the convective influence of the secondary flow on the main flow is essential to a mathematical model of curved channel flow. Models that disregard this effect are at best equivalent to the present one with $k_{sn} = 0$ (cf. figure 7), even if the flow in regions with strong variations of the channel curvature is described more accurately (cf. ref. [17]).

References

1. Van Bendegom, L., Some considerations on river morphology and river improvement (in Dutch), De Ingenieur, 59 (1947), no. 4, p. B1-11.
2. Kuipers, J. and Vreugdenhil, C.B., Calculations of two-dimensional horizontal flow, Delft Hydraulics Laboratory, Report S163, part I (1973).
3. Engelund, F., Flow and bed topography in channel bends, Proc. ASCE, J. Hydr. Div., 100 (1974), no. HY-11, p. 1631-1648.
4. De Vriend, H.J., A mathematical model of steady flow in curved shallow channels, Comm. on Hydraulics, Delft University of Technology, Report 76-1 (1976).
5. De Vriend, H.J., A mathematical model of steady flow in curved shallow channels, J. Hydr. Res., 15, (1977), no. 1, p. 37-54.
6. Sherenkov, I.A. and Gladyshev, M.T., Mathematical modelling of two-dimensional plane flows in open channels, Proc. XVIII-th Congress of the IAHR, Baden-Baden (1977), paper A105.
7. Pratap, V.S., Flow and heat transfer in curved ducts, Imp. Coll. London, Dept. Mech. Eng., Ph.D. thesis HTS/75/25 (1975).
8. Pratap, V.S., and Spalding, D.B., Numerical computations of the flow in curved ducts, Aeron. Quarterly, 26 (1975), part 3, p. 219-228.
9. Leschziner, M. and Rodi, W., Calculation of three-dimensional turbulent flow in strongly curved open channels, Univ. Karlsruhe Sonderforschungsbereich 80, Report SFB80/T/126 (1978).
10. Leschziner, M. and Rodi, W., Calculation of strongly curved open channel flow, Proc. ASCE, J. Hydr. Div., 105 (1979), no. HY10, p. 1297-1314.
11. Rouse, H., Advances Mechanics of Fluids (Appendix A), John Wiley, New York (1959).
12. Yotsukura, N. and Sayre, W.W., Transverse mixing in natural channels, Water Res. Research, 12 (1976), no. 4, p. 695-704.

13. Rozovskii, I.L., Flow of water in bends of open channels, Israel Program for Scientific Translation, Jerusalem (1961).
14. Vanoni, V.A., Transportation of suspended sediment by water, Transactions ASCE, 111 (1946), p. 67-102.
15. Jobson, H.E. and Sayre, W.W., Vertical transfer in open channel flow, Proc. ASCE, J. Hydr. Div., 96, (1970), no. HY3, p. 703-724.
16. De Vriend, H.J. and Koch, F.G., Flow of water in a curved open channel with a fixed plane bed, Delft Hydraulics Laboratory/ Delft University of Technology, TOW-report R657-V/M1415-I (1977).
17. De Vriend, H.J. and Koch, F.G., Flow of water in a curved open channel with a fixed uneven bed, Delft Hydraulics Laboratory/ Delft University of Technology, TOW-report R657-VI/M1415-II (1978).
18. De Vriend, H.J., Accuracy of measurements in a curved open channel, Delft Hydraulics Laboratory/Delft University of Technology, TOW-report R657-VII/M1415-III (1978).

Notations

a	bottom friction and secondary flow convection coeffficient
A	eddy viscosity
b	transverse main flow convection coefficient
C	Chezy-factor
f_1	main flow distribution function
f_2	secondary flow distribution function
g	acceleration due to gravity
h	depth of flow
i,j	point index in the computational grid
k_{sn}	secondary flow convection factor
ℓ_1,ℓ_2	metric factors in the (ψ,ϕ)-system
n	distance along the transverse river coordinate lines
n	distance along the normal lines of the depth-averaged flow field
p	pressure
P	total pressure $p+\rho gz$
Q	discharge
R_s	radius of curvature of the streamlines of the depth-averaged flow
R_n	radius of curvature of the normal lines of the depth averaged flow
R_1	radius of curvature of the s-lines
R_2	radius of curvature of the n-lines
s	distance along the longitudinal river coordinate lines
s	distance along the streamlines of the depth-averaged flow
u_s,u_n,u_z	velocity components in the (s,n,z)-coordinate system
u_s, u_n	velocity components in the streamline coordinate system
z	vertical coordinate
Δn, Δs	mesh sizes in the computational grid
κ	Von Karman's constant
τ_n, τ_s	bottom shear stress components
ψ, ϕ	orthogonal curvilinear coordinates in the horizontal plane.